Inorganic Chemistry
Cite This: Inorg. Chem. 2019, 58, 8111−8119
Article
pubs.acs.org/IC

In Situ Neutron Diffraction Studies of the Metal Flux Growth of Ba/Yb/Mg/Si Intermetallics

Guillermo Vasquez,[†] Ashfia Huq,[‡] and Susan E. Latturner*[,†]

[†]Department of Chemistry and Biochemistry, Florida State University, Tallahassee, Florida 32306, United States
[‡]Neutron Scattering Division, Spallation Neutron Source, Oak Ridge, Tennessee 37831, United States

Supporting Information

ABSTRACT: The Ba/Yb/Mg/Si intermetallic system is extremely complex, with four competing structurally related compounds forming from reactions of barium, ytterbium, and silicon in magnesium-rich Mg/Al flux. In addition to the previously reported $Ba_2Yb_{0.9}Mg_{11.1}Si_7$, $Ba_5Yb_2Mg_{17}Si_{12}$, and $Ba_{20}Yb_5Mg_{61}Si_{43}$, a new compound has been found. $Ba_6Yb_{1.84}Mg_{18.16}Si_{13}$ crystallizes in the $P\bar{6}$ space group, with the $Zr_6Ni_{20}P_{13}$ structure type. Quenching experiments and in situ neutron powder diffraction studies were carried out to determine the reaction parameters that favor particular products. Under slow-cooling conditions, $Ba_5Yb_2Mg_{17}Si_{12}$ precipitates from the flux at 800 °C. A faster cooling rate of an identical reaction results in the formation of single crystals of $Ba_{20}Yb_5Mg_{61}Si_{43}$ in the flux at 640 °C. This indicates that the crystallization of products in this metal flux reaction does not involve precipitation and interconversion of different phases but instead depends on the rate of cooling across the supersaturated metastable zone in this system.

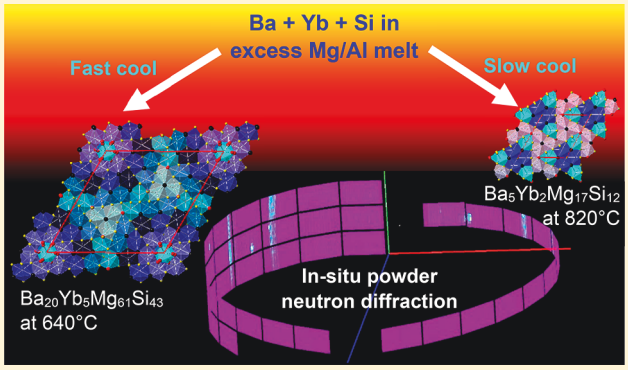

INTRODUCTION

Metal silicides exhibit a wide range of properties ranging from superconductivity (W_5Si_3, V_3Si, Ba_8Si_{46}) and magnetocaloric behavior ($Gd_5Si_2Ge_2$) to high stability and melting point ($TaSi_2$).[1−3] Semiconducting or semimetallic multinary silicides are of particular interest as potential thermoelectric materials. Mg_2Si and substituted derivatives such as $Mg_2Si_{0.4}Sn_{0.6}$ exhibit excellent thermoelectric figures of merit (ZT = 1.2 at 700 K) despite their simple fluorite structure.[4] Zintl phase silicides such as $Ba_8Al_{16}Si_{30}$ and $Ba_{1.9}Ca_{2.4}Mg_{9.7}Si_7$ show promising characteristics, in large part because of their low thermal conductivity that results from complex structures, heavy-element incorporation, and rattling atoms.[5,6] Our recent investigations of the metal flux growth of Ba/Yb/Mg/Si compounds yielded three competing charge-balanced silicide phases ($Ba_2Yb_{0.9}Mg_{11.1}Si_7$, $Ba_5Yb_2Mg_{17}Si_{12}$, and $Ba_{20}Yb_5Mg_{61}Si_{43}$).[7] $Ba_{20}Yb_5Mg_{61}Si_{43}$ is of particular interest as a thermoelectric material due to its semimetallic behavior, large unit cell, structural disorder, and a composition of relatively abundant nontoxic elements.

The formation of competing products is a feature and a drawback of flux reactions, allowing for the discovery of new phases but making isolation in pure form somewhat difficult. The flux synthesis method uses an excess of a low-melting metal or salt as a solvent for other reactants. The formation of a solution eliminates the diffusion barriers inherent in the solid-state synthesis method and enables crystal growth of products if the solution is cooled slowly enough.[8] However, it also allows for formation of different products if reaction parameters (maximum temperature, cooling rate, quench temperature) are varied. The typical way to interrogate this behavior is by running many parallel reactions, modifying one parameter at a time to observe the effects. The advent of in situ diffraction experiments may streamline this process. The "panoramic synthesis" diffraction method, wherein a flux reaction is carried out in a heated sample holder in a diffractometer to enable the observation of phase transformation events, has proven extremely powerful for the detection of intermediate phases that may form and interconvert during heating or cooling of a reaction mixture.[9] Information about such events is vital to understanding and potentially controlling the growth mechanism of desired products; because of this, in situ characterization methods are of great interest as potentially transformative research capabilities.[10] The use of in situ diffraction has been demonstrated for syntheses of complex metal sulfides in polysulfide salt fluxes by Kanatzidis et al.[9,11] It has also been used by the O'Hare and zur Loye groups to study the growth of oxides in Na_2SO_4 and KCl/NaCl fluxes, respectively.[12,13]

In situ diffraction measurements on salt flux reactions have been very informative, but there have been few (if any) reports on similar experiments to explore metal flux reactions. In this work, we used this method to investigate reactions of barium,

Received: March 25, 2019
Published: May 24, 2019

DOI: 10.1021/acs.inorgchem.9b00857
Inorg. Chem. 2019, 58, 8111−8119

ytterbium, and silicon in Mg/Al flux, a system that has yielded three Ba/Yb/Mg/Si products and is highly sensitive to slight perturbations in the cooling profile. This is demonstrated by the fact that further modifications of heating profile lead to formation of a fourth product, $Ba_6Yb_{1.84}Mg_{18.16}Si_{13}$. However, $Ba_5Yb_2Mg_{17}Si_{12}$ and $Ba_{20}Yb_5Mg_{61}Si_{43}$ are the most prevalent products. In situ neutron diffraction data were collected for two sealed ampules containing identical flux reaction components. $Ba_{20}Yb_5Mg_{61}Si_{43}$ crystallized at 640 °C from the reaction cooled in 10 h, and $Ba_5Yb_2Mg_{17}Si_{12}$ formed at 800 °C in the reaction mixture cooled at a slower rate. These results highlight the large metastable zone in the solubility of Ba/Yb/Mg/Si phases in the metal flux and indicate that the mechanism of intermetallic growth from molten metals may be different from that of the salt flux growth of ionic compounds. This information was subsequently used to adjust reaction parameters in the laboratory, which successfully yielded the desired phases reproducibly.

EXPERIMENTAL PROCEDURE

Flux Growth of $Ba_6Yb_{1.84}Mg_{18.16}Si_{13}$. The synthesis is similar to that reported for the three previously reported Ba/Yb/Mg/Si phases.[7] Elements were used as received (magnesium and aluminum slugs, 99.95% and 99.99%, Alfa Aesar; ytterbium chunks, 99.9%, Alfa Aesar; barium rod, 99+%, Alfa Aesar; powdered silicon, 99+%, Strem). These reactants were loaded into a stainless steel crucible under argon in a Mg/Al/Si/Ba/Yb mmol ratio of 21:9:1.5:1.25:0.25. This crucible was welded shut under argon and placed into a quartz jacket that was flame-sealed under vacuum. The ampule was then heated from room temperature to 950 °C in 10 h, held at 950 °C for 10 h, and cooled to 750 °C in 80 h. It was then removed from the furnace, inverted, and centrifuged for 1 min to decant the excess Mg/Al melt. The crucible was cut open, and the crystals adhering to the walls were scraped out. $Ba_6Yb_{1.84}Mg_{18.16}Si_{13}$ is only seen in some cases; reaction mixtures prepared and heated identically were more often found to produce $Ba_{20}Yb_5Mg_{61}Si_{43}$ or $Ba_5Yb_2Mg_{17}Si_{12}$. Other reaction ratios were also explored (such as an Mg/Al/Si/Ba/Yb mmol ratio of 29:1:1.5:1.25:0.25), prepared as described above. Centrifuging temperatures between 700 and 800 °C were investigated; the flux becomes highly viscous at lower temperatures. During processing of identical sets of reaction mixtures heated in the same furnace, it was found that if subsequent reaction ampules were immediately centrifuged after a previous reaction vessel was removed, that ampule would produce no solid, likely due to the temporary oscillation in the furnace temperature causing products to redissolve. The heating profile was therefore modified to include a 2 h holding period at 725 °C between when reaction ampules were removed, which drastically increased the yield of product crystals.

Quenching Experiments. Rapid quenching reactions were carried out in an attempt to eliminate effects of fluctuating furnace temperature during the centrifugation process, as well as to determine possible mmol ratios for in situ neutron diffraction experiments. Reaction mixtures with several different Mg/Al/Si/Ba/Yb ratios were prepared in quartz-jacketed stainless steel crucibles as described above. The ampules were heated from room temperature to 950 °C in 10 h, held at 950 °C for 10 h, and cooled to 725 °C in 10 h. The reaction ampules were then removed from the furnace and immediately quenched in water (a more rapid process than the centrifugation procedure, although the products become embedded in the solidified flux). After cooling, the steel crucibles were sliced horizontally into disks using a 3 in. diameter millimeter width slitting saw and then polished using sandpaper of increasing grit. The disks were then analyzed with a scanning electron microscope using elemental mapping to determine the identity of the products.

Elemental Analysis. Products were analyzed by SEM-EDS using a FEI Nova 400 NanoSEM with energy dispersive spectroscopy (EDS) capabilities. Samples of flux-grown product crystals were mounted onto aluminum pucks using double-sided carbon tape and analyzed using a 30 kV acceleration voltage. The surface of the pucks was completely covered with carbon tape to eliminate Al artifacts produced by the puck. For $Ba_6Yb_{1.84}Mg_{18.16}Si_{13}$ crystals, a [16(0.5)]/[4(0.5)]/[48(2)]/[32(1.4)] Ba/Yb/Mg/Si atomic ratio was indicated. Element mapping was carried out on disks sliced from the rapidly quenched reaction mixtures in order to detect what phases were present in the ingot of solidified flux metals and products.

Single-Crystal X-ray Diffraction. Samples of $Ba_6Yb_{1.84}Mg_{18.16}Si_{13}$ were examined under a microscope to select crystals for diffraction studies. Suitable pieces were cut from larger crystals and were mounted in Dual-Thickness MicroLoops (MiTeGen Loop/Mount) using Parabar oil. Single-crystal X-ray diffraction data were collected at 293 K using a Bruker APEX 2 CCD diffractometer with a Mo Kα radiation source. Absorption corrections were applied to the data using the SADABS program. Refinement of the structures were performed using the SHELXTL package.[14,15] The structure was solved in the hexagonal $P\bar{6}$ space group. Crystallographic data and collection parameters for this compound are shown in Table 1.

Table 1. Crystallographic Data Collection Parameters for $Ba_6Yb_{1.84}Mg_{18.16}Si_{13}$

chemical formula	$Ba_6Yb_{1.84(6)}Mg_{18.16(6)}Si_{13}$
molar mass (g/mol)	1949.36
cryst syst, space group	hexagonal, $P\bar{6}$
temp (K)	293
a, c (Å)	15.4554(11), 4.5046(3)
V (Å^3)	931.85(15)
Z	1
radiation type	Mo $K\alpha$
μ (mm^{-1})	11.53
no. of measd, indep, and obsd ($I > 2\sigma(I)$) rflns	10868, 1696, 1690
R_{int}	0.020
2θ values (deg)	$2\theta_{max}$ = 1.521°, $2\theta_{min}$ = 56.948
no. of rflns	1696
no. of params	83
R1, wR2 (all data)[a]	0.0122, 0.0290
R1, wR2 ($I > 2\sigma(I)$)	0.012, 0.029
$\Delta\rangle_{max}$, $\Delta\rangle_{min}$ (e Å^{-3})	0.93, −0.82
absolute structure	refined as an inversion twin
absolute structure param	0.375(13)

[a] $R1 = \sum(|F_o| - |F_c|)/\sum|F_o|$; $wR2 = [\sum[w(F_o^2 - F_c^2)^2]/\sum(w|F_o|^2)^2]^{1/2}$.

Additional crystallographic data, including tables of atom positions and thermal parameters and bond lengths, can be found in Tables S1 and S2 in the Supporting Information and have been deposited as a CIF file.

Powder X-ray Diffraction. The products of flux syntheses were analyzed using a PANalytical X-Pert PRO diffractometer with a Cu Kα radiation source. Powder samples were prepared by grinding bulk samples of solid products isolated from the flux by centrifugation. The resulting patterns were compared to calculated patterns on the basis of Ba/Yb/Mg/Si phase single-crystal structures.

In Situ Neutron Powder Diffraction. To increase the likelihood that neutron diffraction peaks would be observable, quenching reactions were carried out on increasingly concentrated flux reactions. SEM and PXRD on the quenched products indicated that a Mg:Al:Ba:Si:Yb 29:1:3:2.5:0.5 mmol ratio yielded Ba/Yb/Mg/Si quaternary phases in observable amounts. Several batches of this mixture were therefore loaded into stainless steel crucibles under argon. The crucibles were sealed shut by arc welding under argon. Neutron powder diffraction data were collected using the POWGEN (BL-11A) diffractometer at the Spallation Neutron Source (SNS) at Oak Ridge National Laboratory.[16] For each neutron diffraction experiment, a steel reaction ampule was placed inside a 10 mm inner

DOI: 10.1021/acs.inorgchem.9b00857
Inorg. Chem. 2019, 58, 8111−8119

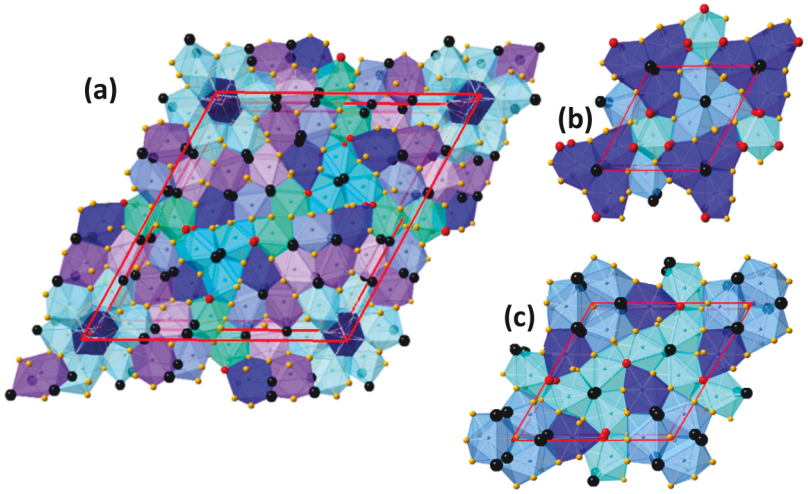

Figure 1. Structures of Ba/Yb/Mg/Si compounds grown in Mg/Al flux, viewed down the *c* axis: (a) $Ba_{20}Yb_5Mg_{61}Si_{43}$ structure ($Ho_{20}Ni_{66}P_{43}$ type, $P6_3/m$) with eight unique silicon sites; (b) $Ba_2Yb_{0.9}Mg_{11.1}Si_7$ structure ($Zr_2Fe_{12}P_7$ type, $P\bar{6}$) with three unique silicon sites; (c) $Ba_5Yb_2Mg_{17}Si_{12}$ structure ($Ho_5Ni_{19}P_{12}$ type, $P\bar{6}2m$) with three unique silicon sites. Ba sites are in black, Yb/Mg mixed sites are in red, Mg sites are in yellow, and Si sites are in blue; Si@$(Ba/Yb/Mg)_9$ tricapped trigonal prism building blocks are shown as blue polyhedra.

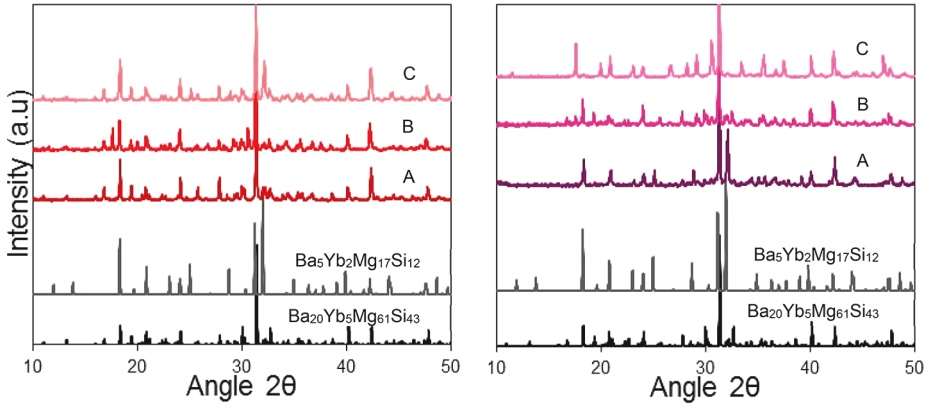

Figure 2. Powder X-ray diffraction data for solid products of two series (series 1 on left, series 2 on right) of three flux reactions of Ba, Yb, and Si in Mg/Al flux run in parallel, all with Mg:Al:Si:Ba:Yb mmol ratio of 29:1:1.5:1.25:0.25. Calculated patterns derived from the $Ba_{20}Yb_5Mg_{61}Si_{43}$ and $Ba_5Yb_2Mg_{17}Si_{12}$ crystal structures are in black and gray, while the data for the powdered product are in shades of red and purple.

diameter vanadium sample can with a boron nitride lid. The vanadium can was then loaded into the MICAS vacuum furnace at POWGEN. Data were collected on two samples.

In the first experiment, the first sample was heated to 950 °C at 2 °C/min, held at 950 °C for 10 h, and then cooled to 500 °C at 1 °C/min. Diffraction data were collected with a wavelength center of 2.665 Å throughout the heating, dwell, and cooling process using the time event mode data collection at SNS; this allows postprocessing of the data as described in a previous report.[17] In the second experiment, 1 or 2 h soaks were introduced during the cooling process to allow for more data collection at specific temperatures. The second sample was heated to 950 °C at 4 °C/min, held at 950 °C for 5 h, and then cooled from 950 °C at a rate of 1 °C/min to soak temperatures of 900, 820, 750, 725, 700, 675, 650, 625, 600, 575, and 550 °C. The cooling was halted for 1 h hold times at 900, 820, 750, 725, 700, 675, and 550 °C and 2 h hold times at 650, 625, 600, and 575 °C. Diffraction data were collected with a wavelength center of 2.665 Å (covering a *d* spacing of 1.1−20 Å) throughout the heating, dwell, and cooling process.

RESULTS AND DISCUSSION

Metal flux synthesis of intermetallics has proven to be a fruitful method for discovery and crystal growth of new materials. However, the mechanism of flux reactions is not understood, and the reaction outcomes are therefore difficult to predict or control. Many metal flux systems yield competing products that are structurally related, containing similar building blocks assembled in different patterns.[18] Examples of such systems include the Ce_nPdIn_{3n+2} homologous series (grown in indium flux), the Ce/Pd/Ga system (grown in Ga flux), and the formation of tetragonal $La_6M_{13}Sn$ and $La_{11}M_{13}Sn_{4-d}$ (M = Mn/Ni/Al) phases grown in La/Ni flux.[19−21] We recently reported three competing Ba/Yb/Mg/Si semimetallic silicides formed from reactions in Mg/Al fluxes (Figure 1).[7] In our continuing exploration of this system, a fourth phase has been discovered.

The Ba/Yb/Mg/Si compounds initially reported include $Ba_2Yb_{0.9}Mg_{11.1}Si_7$, $Ba_5Yb_2Mg_{17}Si_{12}$, and $Ba_{20}Yb_5Mg_{61}Si_{43}$, with the last two being the predominant products. All three compounds exhibit hexagonal crystal structures that are analogous to those of ternary metal phosphides ($Zr_2Ni_{12}P_7$, $Ho_5Ni_{19}P_{12}$, and $Ho_{20}Ni_{66}P_{43}$, respectively). All of the structures feature silicon anions surrounded by nine divalent cations in tricapped-trigonal-prismatic coordination; see Figure 1. $Ba_{20}Yb_5Mg_{61}Si_{43}$ is of particular interest as a potential thermoelectric material, due to its large unit cell, disorder in

DOI: 10.1021/acs.inorgchem.9b00857
Inorg. Chem. 2019, 58, 8111−8119

the form of site mixing and splitting, heavy atoms, and charge-balanced semimetallic nature. In attempts to optimize the synthesis of this product, a reaction ratio of 29:1:1.5:1.25:0.25 mmol heated from room temperature to 950 °C in 10 h, held at 950 °C for 10 h, and cooled to 725 °C in 10 h would produce the desired compound in good yield and purity. However, subsequent attempts to reproduce these results and scale up the product by running identical reactions in parallel resulted in several reaction vessels yielding no product. It was observed that, when the initial reaction ampule was removed from the furnace for centrifugation, the furnace would then oscillate in temperature to restabilize at 725 °C. The temporary increase in temperature may cause products in other reaction ampules to redissolve into the molten flux; when they were centrifuged a few minutes later, no solid products could be isolated. To circumvent this issue, a 2 h holding period at 725 °C between taking out reaction ampules was implemented, increasing the yield of products obtained. However, even though crystals were obtained, the phases that were produced would vary, as can be seen with powder diffraction data shown in Figure 2. $Ba_{20}Yb_5Mg_{61}Si_{43}$ was the most commonly observed product (all of series 1, and reaction 2B); however, several of these reactions yielded $Ba_5Yb_2Mg_{17}Si_{12}$ (reaction 2A; also see Figure S1 in the Supporting Information). One of them produced the new $Ba_6Yb_{1.84}Mg_{18.16}Si_{13}$, evidenced by the powder pattern that did not match the expected reference patterns (reaction 2C). Single crystals from this reaction were then analyzed to determine the structure of the new product. The powder pattern is compared to the calculated pattern for the $Ba_6Yb_{1.84}Mg_{18.16}Si_{13}$ structure in Figure S2.

Structure of $Ba_6Yb_{1.84}Mg_{18.16}Si_{13}$. $Ba_6Yb_{1.84}Mg_{18.16}Si_{13}$ has the $Zr_6Ni_{20}P_{13}$ structure type in the hexagonal space group $P\bar{6}$, shown in Figure 3.[22] The silicon anions occupy the

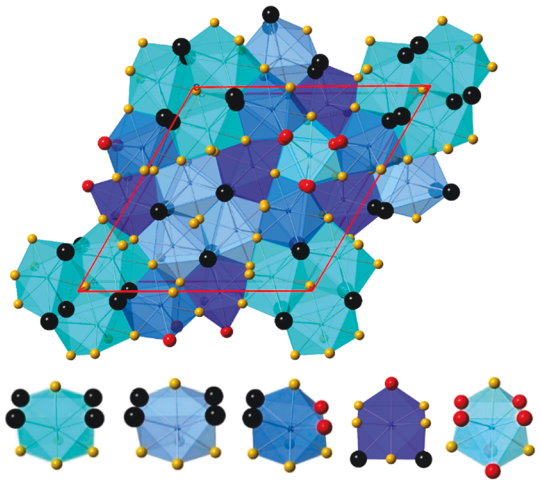

Figure 3. $Ba_6Yb_{1.84}Mg_{18.16}Si_{13}$ structure viewed down the *c* axis and coordination of the five unique silicon sites shown as blue tricapped-trigonal-prism polyhedra. The Yb/Mg mixed sites are in red, Mg sites are in yellow, Ba sites are in black, and Si sites are in blue.

phosphorus sites of the parent structure, barium cations occupy the zirconium sites, and magnesium and ytterbium cations are positioned on the nickel sites. There are five crystallographically unique Si anion sites, each of which is surrounded by nine alkaline-earth and rare-earth anions ($Si@(Ba,Yb,Mg)_9$). The Ba–Si bond lengths (3.454(1)–3.505(1) Å) in these tricapped trigonal prisms are within the range of previously reported Ba–Si bond lengths (3.3729–3.7653 Å) in $BaSi_2$.[23] The Mg–Si bond lengths (2.673(3)–3.100(1) Å) are shorter, and similar to those in Mg_2Si (2.7657 Å) and $Ba_{1.9}Ca_{2.4}Mg_{9.7}Si_7$ (2.734(1)–2.903(1) Å).[24,6] There is only one disordered site, which is occupied by a mix of ytterbium and magnesium. The site is a 3j Wyckoff site, which refines as 61.2% Yb/38.8% Mg. The distance between this mixed site and neighboring silicon sites (2.673(3)–3.100(1) Å) is similar to Yb–Si distances reported for $YbSi_2$ (2.896–2.9898 Å) but are too short to accommodate barium and longer than Mg–Si bonds reported for Mg_2Si (2.7657 Å).[24,25] $Ba_6Yb_{1.84}Mg_{18.16}Si_{13}$ is part of a homologous series with $Ba_2Yb_{0.9}Mg_{11.1}Si_7$ and $Ba_{20}Yb_5Mg_{61}Si_{43}$. Similar to the analysis of their phosphide parent structures, these Ba/Yb/Mg/Si stoichiometries are expressed by the formula $Ba_{n(n-1)}(Yb/Mg)_{(n+1)(n+2)}Si_{n(n+1)+1}$, with n = 2, 3, 6; they feature triangular substructures which increase in complexity as n rises, as described in refs 26 and 27.

$Ba_6Yb_{1.84}Mg_{18.16}Si_{13}$ exhibits roughly temperature independent susceptibility, indicating it is Pauli paramagnetic, similar to the behavior of the other Ba/Yb/Mg/Si compounds (see Figure 4). This confirms that the ytterbium ions in this phase

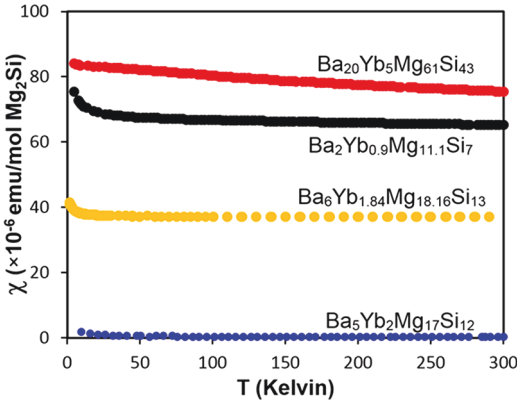

Figure 4. Temperature dependence of the magnetic susceptibility for $Ba_6Yb_{1.84}Mg_{18.16}Si_{13}$ collected with an applied field of 3000 G, compared to data previously reported for other Ba/Yb/Mg/Si compounds.

are divalent; given the 2:1 ratio of divalent cations (Ba^{2+}, Mg^{2+}, and Yb^{2+}) to Si^{4-} anions, it is therefore a charge-balanced Zintl phase and is expected to be a small band gap semiconductor or semimetal. The magnitude of the Pauli paramagnetism is roughly 3.8×10^{-5} emu/mol M_2Si, normalized to the 2:1 M_2Si formula unit. This is higher than that of $Ba_5Yb_2Mg_{17}Si_{12}$ (3.0×10^{-7} emu/mol M_2Si) but lower than those of $Ba_{20}Yb_5Mg_{61}Si_{43}$ and $Ba_2Yb_{0.9}Mg_{11.1}Si_7$ (7.8×10^{-5} and 6.6×10^{-5} emu/mol M_2Si, respectively). The low value of the susceptibility (in comparison to other Pauli paramagnetic metal silicides such as $Yb(Zn,Si)_2$ and $YbZn_2Si_2$, which have moments in the 10^{-3} emu/mol range)[28] is likely due to a low density of states at the Fermi level for these charge-balanced, semimetallic Ba/Yb/Mg/Si Zintl phases. $Ba_{20}Yb_5Mg_{61}Si_{43}$ has the highest susceptibility, indicating that the phase has more electronic states at E_F and will exhibit more metallic characteristics than the other phases, whereas $Ba_5Yb_2Mg_{17}Si_{12}$ has the lowest susceptibility, indicating the phase likely has fewer electronic states at E_F and will exhibit lower conductivity. All of these compounds exhibit a pseudogap in the density of states at the

DOI: 10.1021/acs.inorgchem.9b00857
Inorg. Chem. 2019, 58, 8111–8119

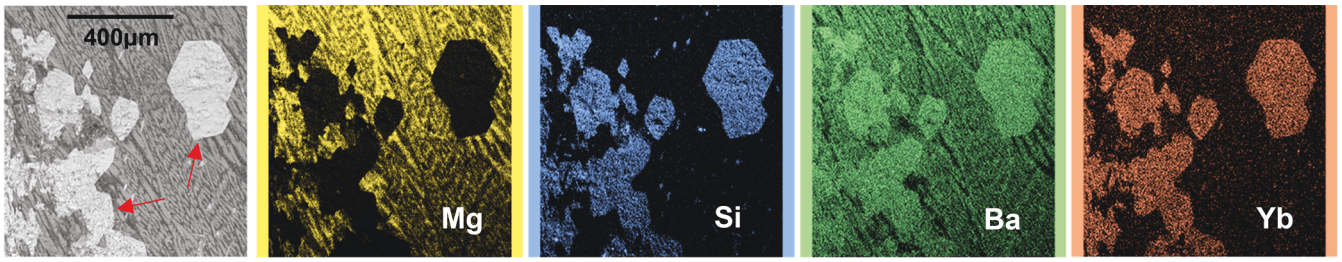

Figure 5. SEM-EDX mapping of a disk cut from a reaction mixture of Mg/Al/Si/Ba/Yb with a mmol ratio of 29:1:2.5:3:0.5. The first image is an SEM-EDS image of the selected area of interest. Subsequent elemental maps for magnesium, silicon, barium, and ytterbium are respectively indicated in yellow, blue, green, and orange.

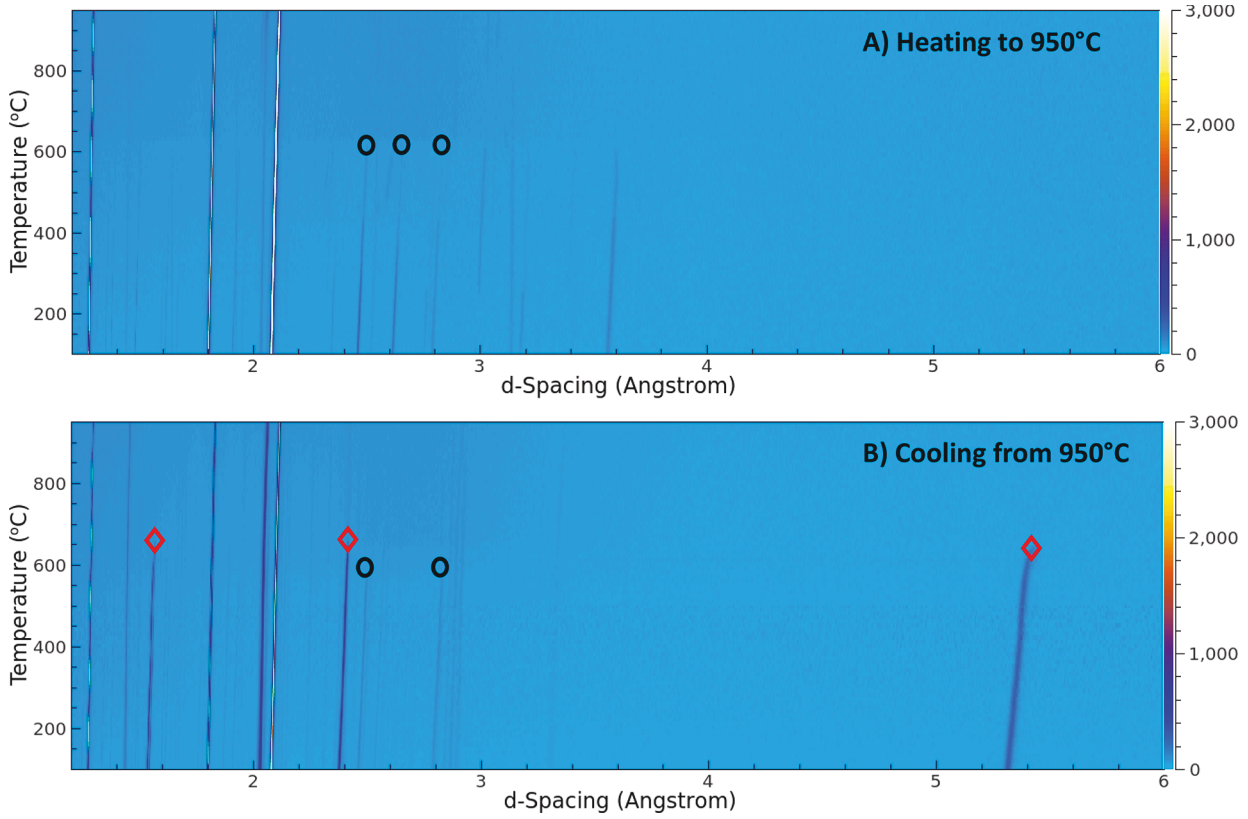

Figure 6. Temperature dependence of neutron diffraction data for a reaction of Mg/Al/Ba/Si/Yb with a 29:1:2.5:3:0.5 mmol ratio in a steel ampule (sample 1, fast cooling): (a) 2D plot of data collected during heating; (b) 2D plot of data collected during cooling. Disappearance and reappearance of magnesium peaks are indicated by black circles. $Ba_{20}Yb_5Mg_{61}Si_{43}$ diffraction peaks appearing during cooling are highlighted with red symbols.

Fermi level between filled silicon bands just below E_F and magnesium bands just above E_F (see ref 7 and Figure S3 in the Supporting Information).

Quenching Experiments. Given the competing phases in this system, in situ diffraction data collected during cooling were needed to shed light on the precise temperature at which the compounds form. X-ray diffraction studies were not feasible because the Mg/Al flux will attack the thin quartz capillaries typically used. The greater penetration depth of neutrons, on the other hand, allows for diffraction from larger samples in sealed steel ampules and is particularly beneficial for flux reactions that are carried out in an excess of molten metal. Quenching experiments were carried out to determine a suitable reaction stoichiometry to use during these neutron diffraction experiments. SEM elemental mapping images of disks cut from quenched reactions of different concentrations of Ba, Si, and Yb in a Mg/Al flux are shown in Figure 5 and Figures S4 and S5 in the Supporting Information. All of the reactions show particles of Ba/Yb/Mg/Si quaternary phases surrounded by a Mg-rich matrix. Of the three reaction ratios explored in this manner, the "intermediate" concentration of Mg/Al/Si/Ba/Yb with a mmol ratio of 29:1:2.5:3:0.5, shown in Figure 5, was found to be the most suitable to use in the subsequent neutron diffraction experiment.

The first image in Figure 5 is an SEM-EDS image of the selected area of the disk cut from the reaction ampule. The image has distinct features: large hexagonal areas (indicated by arrows) and smaller circular particulates, all embedded in a larger dark gray striated matrix. The magnesium mapping (in yellow) indicates that the matrix is much richer in magnesium than the embedded features; this is understandable, considering that a high concentration of Mg was used in the flux. The

DOI: 10.1021/acs.inorgchem.9b00857
Inorg. Chem. 2019, 58, 8111−8119

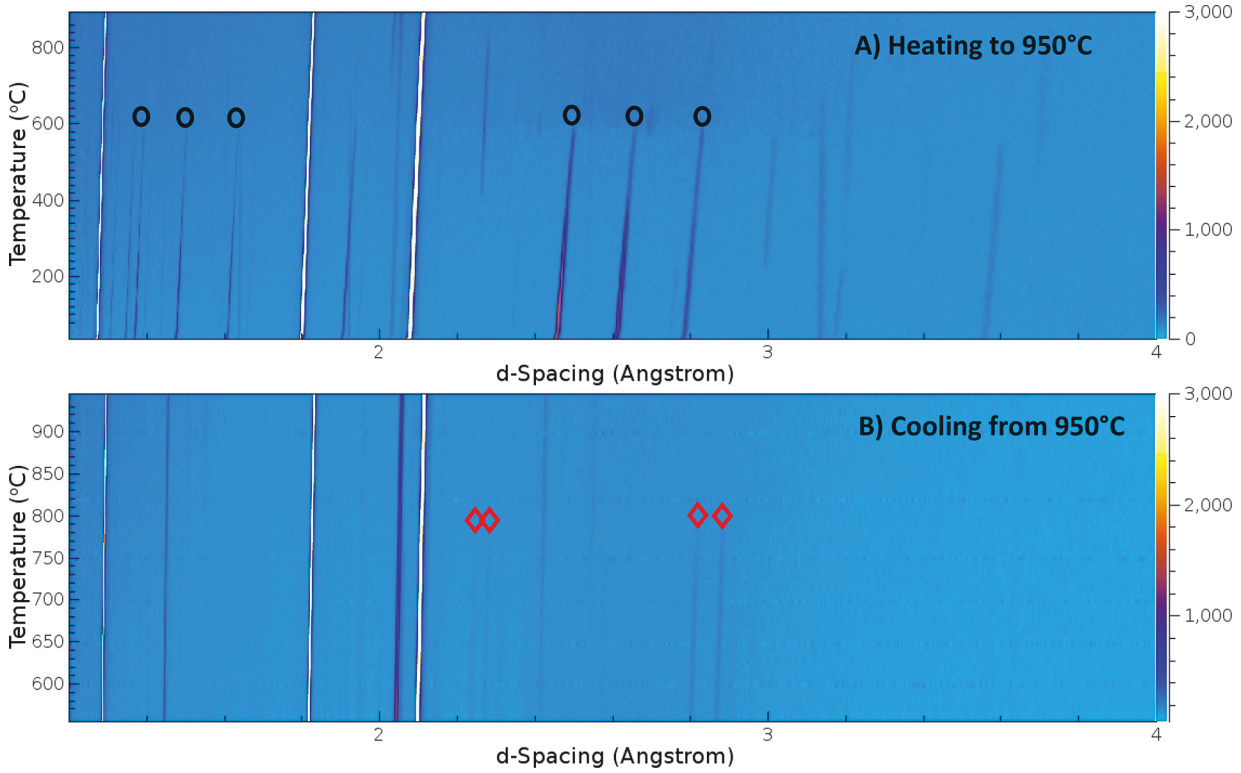

Figure 7. Temperature dependence of neutron diffraction data for a reaction of Mg/Al/Ba/Si/Yb with a 29:1:2.5:3:0.5 mmol ratio in a steel ampule (sample 2, slow cooling): (a) 2D plot of data collected during heating; (b) 2D plot of data collected during cooling. Magnesium peaks are indicated by black circles. $Ba_5Yb_2Mg_{17}Si_{12}$ diffraction peaks appearing during cooling are highlighted with red symbols.

silicon mapping (in blue) reveals that this element is most prominent in the large hexagonal areas and the small circular areas. Barium concentration is indicated in green. Like silicon, the barium is most prominent in the large hexagonal shapes and the small spots. Barium is also present in the light striations of the matrix. The lamellar microstructure of the matrix is characteristic of the solidification of a eutectic mixture.[29] It therefore appears that, at the end of the reaction, the remaining flux composition is close to the eutectic between Mg and Ba_2Mg_{17}, segregating into lamellae of these compounds upon freezing.[30] The ytterbium mapping (in orange) shows that, like silicon and barium, ytterbium is most prominently located in the large hexagonal shapes; however, it is does not seem to appear in the spots or the matrix. The large hexagonal shapes contained all four elements that make up the hexagonal phases. SEM-EDS was conducted on those locations, indicating that the hexagonal shapes have atomic ratios of Ba 16.6(0.5)%, Yb 3.7(2.0)%, Mg 44.9(4.0)%, and Si 34.5(2.1)%. This disk therefore represents precipitation of a Ba/Yb/Mg/Si quaternary phase with ratios indicative of $Ba_{20}Yb_5Mg_{61}Si_{43}$, surrounded by a Ba/Mg matrix. The other two quenched reaction concentrations also showed Ba/Yb/Mg/Si precipitates in a Ba/Mg matrix, but the lower concentration reaction had a lower yield, and the higher concentration reaction indicated attack on the crucible and incorporation of iron in some byproducts (see Figures S4 and S5 in the Supporting Information).

In Situ Neutron Diffraction. Two identically prepared samples (Mg/Al/Ba/Si/Yb with a 29:1:2.5:3:0.5 mmol ratio in welded steel ampules) were used in neutron diffraction experiments on the POWGEN diffractometer at ORNL. For the first sample, data were continuously collected as the sample was heated to 950 °C at 2 °C/min, held at this temperature for 10 h, and then cooled to 500 °C at 1 °C/min; data are shown in Figure 6. While all patterns are dominated by the diffraction due to the steel crucible (very strong austenite lines at d spacings of 1.30, 1.83 , and 2.12 Å; weaker line at d = 2.06 Å from ferrite), diffraction peaks from reactants and products are observable. The initial patterns clearly show the presence of the dominant peaks from magnesium (d = 2.45, 2.60, 2.77 Å; weaker lines at 1.60, 1.47, 1.37, 1.34 Å), barium (3.6 Å), and silicon (1.9, 3.14 Å) reactants. Ytterbium metal is observed to undergo a previously reported transition from fcc (peak at d = 3.19 Å) to hcp (d = 3.02 Å) at 260 °C.[31]

Upon heating, all of the peaks except for those from the steel disappear at 700 °C, with the Mg and Ba peaks disappearing earlier at 600 °C. A new peak appears with a d spacing of 2.05 Å at a temperature of 775 °C; this persists during the dwell period and upon cooling. (This is also seen more clearly in the data for the second sample shown in Figure 7, vide infra.) This is likely to correspond to formation of $(Ni_{1-x}Fe_x)Al$ (with CsCl structure; dominant diffraction peak at d = 2.05 Å) forming from the reaction of the steel ampule with aluminum in the flux melt.[32] This phase was not detected in our typical flux reactions, since it is embedded in the ampule walls. Elemental mapping of samples from quenching reactions confirms formation of a $(Ni_{1-x}Fe_x)Al$ phase with atomic percentages of 35(5)/13(5)/52(1) on the inner walls of the crucible (see Figure S6 in the Supporting Information). Aside from the appearance of these peaks, no other diffraction peaks are noted above 900 °C or during the dwell; this indicates that far shorter dwell times and potentially lower maximum temperatures can be used for these reactions.

DOI: 10.1021/acs.inorgchem.9b00857
Inorg. Chem. 2019, 58, 8111−8119

During the cooling process, three peaks at d = 5.42, 2.42, 1.57 Å appear at 640 °C, just before the reappearance of the magnesium peaks (2.49 and 2.82 Å) as the flux solidifies at 550 °C. The lowered melting point with respect to pure Mg is likely due to eutectic formation. As cooling is continued to room temperature, all of these peaks are observed to shift to lower d spacing, as expected due to thermal contraction. The room-temperature d spacing values of peaks corresponding to the multinary product are 5.3170, 2.3811, and 1.5402 Å. The only phase in the Ba/Yb/Mg/Si system with corresponding diffraction peaks is $Ba_{20}Yb_5Mg_{61}Si_{43}$; these d spacings result from the (1 4 0), (5 5 1), and (3 13 1) planes, respectively. It is notable that these are expected to be weaker reflections, and the pattern is missing the stronger reflections such as (1 7 1) peak with a d spacing of 2.848 Å. Further light was shed on this by looking at the POWGEN individual detector images (see Figure S7 in the Supporting Information), which show diffraction spots instead of lines, indicating that the $Ba_{20}Yb_5Mg_{61}Si_{43}$ is growing from the flux as crystals instead of randomly oriented polycrystalline powder. This will lead to preferred orientation effects, and many of the expected diffraction peaks will likely be out of the range of the POWGEN ring of detectors. Nonetheless, the presence of these peaks indicates that $Ba_{20}Yb_5Mg_{61}Si_{43}$ did form in the flux, crystallizing at a temperature of 640 °C.

For the second sample, the heating and dwell steps were shorter (heating at 4 °C/min and dwelling for only 5 h), and the cooling ramp was longer and was carried out in steps to soak at various temperatures (see Experimental Procedure); the data are shown in Figure 7. Diffraction from the steel crucible was again dominant, and the $(Ni_{1-x}Fe_x)Al$ phase also formed at high temperature. As was the case with the previous sample, peaks from Mg, Si, and Ba reactants were apparent at room temperature, disappearing at 600 °C. Just below this temperature, faint peaks at d = 2.28, 3.20, 3.71 Å appear and then disappear at 850 °C; these likely correspond to formation and then dissolution of Mg_2Si. Upon cooling, several peaks appeared at 800 °C that indicate the precipitation of $Ba_5Yb_2Mg_{17}Si_{12}$. The peaks at d = 2.8778, 2.8134, 2.2761, 2.2425 Å correspond respectively to diffraction from the (2 2 1), (1 3 1), (0 0 2), and (0 5 1) planes in this structure; these are expected to be the strongest diffraction lines for this compound.

These data indicate that sample 1 produced $Ba_{20}Yb_5Mg_{61}Si_{43}$, which precipitated at 640 °C, and sample 2 yielded $Ba_5Yb_2Mg_{17}Si_{12}$, which precipitated at 800 °C. This behavior is contrary to our expectations that phases would form and then interconvert as the temperature changed. That hypothesis was based on what has been observed in salt flux reactions. In situ studies reported for such systems often indicate a cascade of compounds, with each product forming at a specific temperature range and then disappearing, at which point another phase solidifies. For instance, reactions of Bi_2O_3, TiO_2, Fe_2O_3, and Cr_2O_3 in an excess of Na_2SO_4 flux form the initial n = 3 Aurivillius phase $Bi_4Ti_3O_{12}$, which is then observed to convert into the n = 4 substituted variant $Bi_5Ti_3Fe_{0.5}Cr_{0.5}O_{15}$.[12] The reaction of MoO_3 and La_2O_3 with zinc in a CsCl/NaCl eutectic melt sequentially forms $La_2(MoO_4)_3$, then La_2MoO_6, then finally $La_4Mo_2O_{11}$.[13] Similarly, reactions of copper in excess K_2S_3 yield KCu_3S_2 and then $K_3Cu_4S_4$ on heating to 600 °C, followed by formation of $K_3Cu_8S_6$ upon cooling.[11]

Both of the metal flux reactions studied here were prepared as identically as possible, so the large divergence in results (in the absence of external perturbations such as temperature fluctuations caused by opening and closing of a furnace door) is surprising. Variation in cooling rate is the clear distinction between these reactions. Results seem to bracket what is probably the Ostwald–Miers (metastable) region for formation of Ba/Yb/Mg/Si products in this molten solution.[33] This is the supersaturated region, between the highest expected temperature of precipitation (where the solution is saturated) and a more heavily supersaturated point at lower temperature. The temperature range of this supersaturated metastable region (highest expected precipitation temperature vs lowest observed precipitation temperature) for high-temperature solutions such as molten metals has been reported to be as large as 100 °C.[33] Large metastable regions occur when the formation of high local solute concentrations can be avoided (which prevents nucleation and subsequent crystal growth). It is therefore maximized in systems with a small solution volume, a high viscosity solution, and high complexity of the crystallizing substance, all of which are present in this case.

With slow cooling, giving a longer time for equilibrium nucleation processes, $Ba_5Yb_2Mg_{17}Si_{12}$ precipitates at the high-temperature end of this region, around 800 °C. With faster cooling, the system exists in a metastable supersaturated state until $Ba_{20}Yb_5Mg_{61}Si_{43}$ precipitates at 640 °C. To test this, identical reaction mixtures were prepared, heated to 950 °C in 10 h, and held at 950 °C for 10 h. One ampule was cooled to 750 °C in 40 h and then centrifuged; the other was cooled to 725 °C in 20 h and then centrifuged. As seen in Figure 8, the more slowly cooled reaction mixture yielded the $Ba_5Yb_2Mg_{17}Si_{12}$ product, and the more quickly cooled reaction mixture yielded $Ba_{20}Yb_5Mg_{61}Si_{43}$.

CONCLUSIONS

Growth of multinary intermetallics in metal flux media is a highly productive synthesis method. However, the reaction mechanisms at play and the effects of various parameters are not well understood, and the reactions can often produce several competing phases or be hindered by a lack of

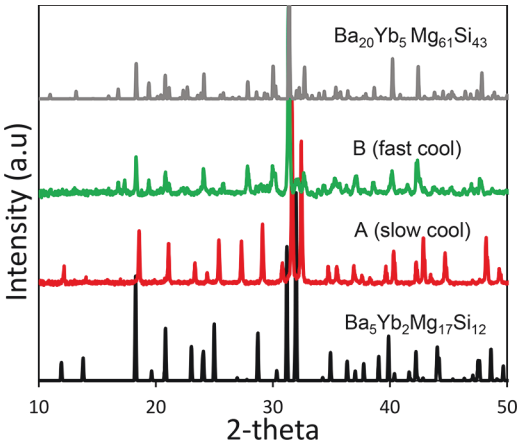

Figure 8. Powder X-ray diffraction data for solid products of reactions of Ba, Yb, and Si in Mg/Al flux. Calculated patterns for $Ba_{20}Yb_5Mg_{61}Si_{43}$ and $Ba_5Yb_2Mg_{17}Si_{12}$ are in grey and black respectively, while the data for identically prepared reactions with slow cooling (A) or fast cooling (B) are given in red and green, respectively.

DOI: 10.1021/acs.inorgchem.9b00857
Inorg. Chem. 2019, 58, 8111–8119

reproducibility. This is very much the case with the Ba/Yb/Mg/Si compounds grown from magnesium/aluminum flux. Four products have been identified thus far: $Ba_2Yb_{0.9}Mg_{11.1}Si_7$, $Ba_6Yb_{1.84}Mg_{18.16}Si_{13}$, $Ba_5Yb_2Mg_{17}Si_{12}$, and $Ba_{20}Yb_5Mg_{61}Si_{43}$. All are comprised of similar building blocks assembled into related hexagonal structures. $Ba_5Yb_2Mg_{17}Si_{12}$ and $Ba_{20}Yb_5Mg_{61}Si_{43}$ are the most prevalent, with the former being the more thermodynamically stable of the two products, as might be expected from its simpler structure. It crystallizes from the flux upon slow cooling to 800 °C. $Ba_{20}Yb_5Mg_{61}Si_{43}$, on the other hand, appears to form from a more supersaturated solution with fast cooling to 640 °C. The other two products ($Ba_2Yb_{0.9}Mg_{11.1}Si_7$ and $Ba_6Yb_{1.84}Mg_{18.16}Si_{13}$) were not observed in the reactions studied in situ; these phases might form under rare and difficult to reproduce conditions involving temperature fluctuations (such as those caused by opening the furnace door) that position the reaction at a specific point in the metastable zone.

It is notable that this system does not involve formation of intermediate phases or yield extensive mixing of products, as might be expected if the formation of these Ba/Yb/Mg/Si compounds involved solid/liquid reactions or solid-to-solid structural transformations. Instead, this system appears to be driven by the dependence of solubility equilibria on temperature. This sets it apart from salt flux reaction chemistry, which quite often involves cascades of intermediates leading to a final product. Further in situ studies on other metal flux systems are needed to see if this is a consistent factor that distinguishes the growth of intermetallics from the formation of more ionic compounds from salt fluxes. The use of neutron diffraction is particularly appealing, since it allows for data collection on laboratory-scale reaction mixtures (contrasted with the requirement of very narrow capillary sample holders for X-ray diffraction). Characterization techniques that interrogate the soluble building blocks which exist in the solution (such as PDF analysis on the melts) will be crucial to further understanding the reaction mechanism. Calculations of relative energies of possible products would also be very useful to shed further light on these complex phenomena.

■ ASSOCIATED CONTENT

Supporting Information

The Supporting Information is available free of charge on the ACS Publications website at DOI: 10.1021/acs.inorgchem.9b00857.

Tables of atomic positions and thermal parameters of $Ba_6Yb_{1.84}Mg_{18.16}Si_{13}$, powder X-ray diffraction data of products of flux reactions, density of states data for Ba/Yb/Mg/Si phases, SEM-EDS images and element mapping of quenched reactions, and POWGEN detector images (PDF)

Accession Codes

CCDC 1905562 contains the supplementary crystallographic data for this paper. These data can be obtained free of charge via www.ccdc.cam.ac.uk/data_request/cif, or by emailing data_request@ccdc.cam.ac.uk, or by contacting The Cambridge Crystallographic Data Centre, 12 Union Road, Cambridge CB2 1EZ, UK; fax: +44 1223 336033.

■ AUTHOR INFORMATION

Corresponding Author

*E-mail for S.E.L.: latturner@chem.fsu.edu).

ORCID

Susan E. Latturner: 0000-0002-6146-5333

Notes

The authors declare no competing financial interest.

■ ACKNOWLEDGMENTS

This research was supported by the Division of Materials Research of the National Science Foundation (grants DMR-14-10214 and DMR-18-08471). This work made use of scanning electron microscope equipment of the Biological Sciences Imaging Resource (BSIR) in the Florida State University Department of Biology; we thank Dr. Eric Lochner for guidance with this instrument. A portion of this research used resources at the Spallation Neutron Source, a DOE Office of Science User Facility operated by Oak Ridge National Laboratory. We thank Dr. Vicky Lynch and Dr. Christina Hoffmann (ORNL) for informative discussions on visualizing the single-crystal diffraction data obtained during the experiment.

■ REFERENCES

(1) Kawashima, K.; Muranaka, T.; Kousaka, Y.; Akutagawa, S.; Akimitsu, J. Superconductivity in Transition Metal-Silicide W_5Si_3. *J. Phys.: Conf. Ser.* **2009**, *150*, No. 052106.

(2) Pecharsky, A. O.; Gschneidner, K. A.; Pecharsky, V. K. The Giant Magnetocaloric Effect of Optimally Prepared $Gd_5Si_2Ge_2$. *J. Appl. Phys.* **2003**, *93* (8), 4722−4728.

(3) Milanese, C.; Buscaglia, V.; Maglia, F.; Anselmi-Tamburini, U. Reactive Growth of Tantalum Silicides in Ta-Si Diffusion Couples. *J. Phys. Chem. B* **2002**, *106*, 5859−5863.

(4) Macario, L. R.; Cheng, X.; Ramirez, D.; Mori, T.; Kleinke, H. Thermoelectric Properties of Bi-Doped Magnesium Silicide Stannides. *ACS Appl. Mater. Interfaces* **2018**, *10*, 40585−40591.

(5) Tsujii, N.; Roudebush, J. H.; Zevalkink, A.; Cox-Uvarov, C. A.; Snyder, G. J.; Kauzlarich, S. E. Phase stability and chemical composition dependence of the thermoelectric properties of the type 1 clathrate $Ba_8Al_xSi_{46-x}$. *J. Solid State Chem.* **2011**, *184*, 1293−1303.

(6) Silsby, K.; Sui, F.; Ma, X.; Kauzlarich, S. M.; Latturner, S. E. Thermoelectric Properties of $Ba_{1.9}Ca_{2.4}Mg_{9.7}Si_7$: A New Silicide Zintl Phase with the $Zr_2Fe_{12}P_7$ Structure Type. *Chem. Mater.* **2015**, *27* (19), 6708−6716.

(7) Vasquez, G.; Latturner, S. E. Metal flux growth of complex alkaline earth/rare earth metal silicides with a homologous series of metal phosphide structure types. *Chem. Mater.* **2018**, *30*, 6478−6485.

(8) Kanatzidis, M. G.; Pöttgen, R.; Jeitschko, W. The Metal Flux: A Preparative Tool for the Exploration of Intermetallic Compounds. *Angew. Chem., Int. Ed.* **2005**, *44* (43), 6996−7023.

(9) Kanatzidis, M. G. Discovery-Synthesis, Design, and Prediction of Chalcogenide Phases. *Inorg. Chem.* **2017**, *56*, 3158−3173.

(10) De Yoreo, J. *Basic Research Needs for Synthesis Science*; Report of the Basic Energy Sciences Workshop on Synthesis Science for Energy Relevant Technology, 2016.

(11) Shoemaker, D. P.; Hu, Y. J.; Chung, D. Y.; Halder, G. J.; Chupas, P. J.; Soderholm, L.; Mitchell, J. F.; Kanatzidis, M. G. In situ studies of a platform for metastable inorganic crystal growth and materials discovery. *Proc. Natl. Acad. Sci. U. S. A.* **2014**, *111*, 10922−10927.

(12) Moorhouse, S. J.; Wu, Y.; Buckley, H. C.; O'Hare, D. Time resolved in situ powder X-ray diffraction reveals the mechanisms of molten salt synthesis. *Chem. Commun.* **2016**, *52*, 13865.

(13) Abeysinghe, D.; Huq, A.; Yeon, J.; Smith, M. D.; Zur Loye, H. C. In Situ Neutron Diffraction Studies of the Flux Crystal Growth of the Reduced Molybdates $La_4Mo_2O_{11}$ and $Ce_4Mo_2O_{11}$: Revealing Unexpected Mixed-Valent Transient Intermediates and Determining

DOI: 10.1021/acs.inorgchem.9b00857
Inorg. Chem. 2019, 58, 8111−8119

the Sequence of Events during Crystal Growth. *Chem. Mater.* **2018**, *30* (3), 1187−1197.
(14) *SAINT, Version 6.02a*; Bruker AXS: Madison, WI, 2000.
(15) Sheldrick, G. M. *SHELXTL NT/2000, Version 6.1*; Bruker AXS: Madison,WI, 2000.
(16) Huq, A.; Hodges, J. P.; Gourdon, O. A.; Heroux, L. POWGEN: A third-generation high resolution high-throughput powder diffraction instrument at the Spallation Neutron Source. *Z. Kristallogr.* **2011**, *1*, 127−135.
(17) Peterson, P. F.; Campbell, S. I.; Reuter, M. A.; Taylor, R. J.; Zikovsky, J. Event-Based Processing of Neutron Scattering Data. *Nucl. Instrum. Methods Phys. Res., Sect. A* **2015**, *803*, 24−28.
(18) Latturner, S. E. Clusters, Assemble: Growth of Intermetallic Compounds from Metal Flux Reactions. *Acc. Chem. Res.* **2018**, *51*, 40−48.
(19) Kratochvilova, M.; Dusek, M.; Uhlirova, K.; Rudajevova, A.; Prokleska, J.; Vondrackova, B.; Custers, J.; Sechovsky, V. Single crystal study of the layered heavy fermion compounds Ce_2PdIn_8, Ce_3PdIn_{11}, Ce_2PtIn_8 and Ce_3PtIn_{11}. *J. Cryst. Growth* **2014**, *397*, 47−52.
(20) Phelan, W. A.; Menard, M. C.; Kangas, M. J.; McCandless, G. T.; Drake, B. L.; Chan, J. Y. Adventures in Crystal Growth: Synthesis and Characterization of Single Crystals of Complex Intermetallic Compounds. *Chem. Mater.* **2012**, *24*, 409−420.
(21) Zaikina, J. V.; Griffin, V.; Latturner, S. E. Switching on a Spin Glass: Flux Growth, Structure, and Magnetism of $La_{11}Mn_{13-x-y}Ni_xAl_ySn_{4-d}$ Intermetallics. *Inorg. Chem.* **2017**, *56*, 15194−15202.
(22) Jean, Y. P.; Guérin, R.; Padious, J.; Sergent, M. Synthesis, Crystal Structures and Properties of $Ho_2Ni_{12}P_7$ and $Ho_6Ni_{20}P_{13}$. *J. Alloys Compd.* **1986**, *118* (2), 191−200.
(23) Evers, J.; Oehlinger, G.; Weiss, A. Solid solutions $M_{1-x}Sr_xSi_2$ (M = Ca, Eu, Ba) and $BaSi_{2-y}Ge_y$ with $SrSi_2$-type structure. *J. Less-Common Met.* **1980**, *69* (2), 399−402.
(24) Saravanan, R.; Robert, M. C. Local Structure of the Thermoelectric Material Mg_2Si Using XRD. *J. Alloys Compd.* **2009**, *479* (1−2), 26−31.
(25) Peter, S. C.; Kanatzidis, M. G. $ThSi_2$ Type Ytterbium Disilicide and Its Analogues YbT_xSi_{2-x} (T = Cr, Fe, Co). *Z. Anorg. Allg. Chem.* **2012**, *638* (2), 287−293.
(26) Pivan, J. Y.; Guerin, R.; Sergent, M. A New Classification Scheme to Describe and Predict Structure Types in Pnictide and Silicide Chemistry. *J. Solid State Chem.* **1987**, *68*, 11−21.
(27) Prots, Y. M.; Jeitschko, W. Lanthanum Nickel Silicides with the General Formula $La_{(n+1)(n+2)}$ $Ni_{n(n-1)+2}Si_{n(n+1)}$ and Other Series of Hexagonal Structures with Metal:Metalloid Ratios Close to 2:1. *Inorg. Chem.* **1998**, *37* (21), 5431−5438.
(28) Grytsiv, A.; Leithe-Jasper, A.; Flandorfer, H.; Rogl, P.; Hiebl, K.; Godart, C.; Velikanova, T. Novel Ytterbium-Zinc-Silicides and Germanides Grown from Zinc-Flux. *J. Alloys Compd.* **1998**, *266* (1−2), 7−12.
(29) Callister, W. D. *Materials Science and Engineering*, 3rd ed.; Wiley: New York, 1994.
(30) Villars, P.; Okamoto, H.; Cenzual, K. *ASM Alloy Phase Diagram Database*; ASM International: 2006−2018.
(31) Bodnar, R. E.; Steinfink, H. Phase Equilibria and Crystal Chemistry of the Intermediate Phases in the Ytterbium-Antimony System. *Inorg. Chem.* **1967**, *6*, 327−330.
(32) Lipson, H.; Taylor, A. Defect Lattices in some Ternary Alloys. *Proc. Royal Soc. London A* **1939**, *173*, 232−237.
(33) Elwell, D.; Scheel, H. J. *Crystal Growth from High Temperature Solutions*; Academic Press: London, 1975 (online ed. with Additional Chapter 11 and Appendices A and B, 2011).

DOI: 10.1021/acs.inorgchem.9b00857
Inorg. Chem. 2019, 58, 8111−8119